Green Synthesis of ZnO/Ag Nanocomposite using *Psidium guajava*: A Study on Characterization and Potential Clinical Application as Advanced Antibacterial Agents on Cotton Bandages

Yasmin Hasna Khairunnisa, Eko Sri Kunarti*, and Nuryono Nuryono

Department of Chemistry, Faculty of Mathematics and Natural Sciences, Universitas Gadjah Mada, Sekip Utara, Yogyakarta 55281, Indonesia

* ***Corresponding author:***

email: eko_kunarti@ugm.ac.id

Received: August 29, 2025
Accepted: December 3, 2025

DOI: 10.22146/ijc.110801

Abstract: *The development of innovative green antibacterial agents has been proposed as a strategy to combat bacterial resistance and improve wound healing. This research explores the synthesis of ZnO/Ag nanocomposites using guava leaf extract and evaluates their antibacterial properties. The study focused on optimizing ZnO nanoparticle synthesis by adjusting precursor concentrations, followed by Ag modification through variations in Ag precursor levels, pH, and reaction times to achieve optimal ZnO/Ag nanocomposites properties. The optimized ZnO and ZnO/Ag materials were applied to cotton bandages, and both the nanomaterials and the coated bandages were characterized using FTIR, SEM, TEM, and UV-vis-NIR, with their antibacterial activity tested against* Staphylococcus aureus *and* Escherichia coli. *The optimal synthesis conditions were identified as 0.60 M ZnO, 1% Ag, 2 h, and pH 12. The characterization results verified the successful synthesis of the ZnO/Ag nanocomposite and its effective coating on cotton bandages. Antibacterial test revealed that the ZnO/Ag demonstrated significantly greater activity than ZnO alone, with inhibition zones measuring 21.35 mm for* S. aureus *and 3.85 mm for* E. coli. *These outcomes highlight the potential of biosynthesized nanomaterials for use in clinical wound dressings to promote wound healing.*

Keywords: *antibacterial; cotton bandages; guava leaf; ZnO/Ag nanocomposite*

■ INTRODUCTION

Enhancing hygiene and infection control has become increasingly critical, particularly through the development of advanced antimicrobial textiles [1]. Bacterial infections remain a significant health concern, with cotton, commonly used in surgical gowns, lab coats, and masks, being highly susceptible to microbial contamination. The challenge has been intensified by the rise of antibiotic- and antimicrobial-resistant bacteria [2]. As reported by Prastiyanto et al. [3], *Escherichia coli*, *Klebsiella pneumoniae*, and *Staphylococcus aureus* are the most commonly identified pathogens in wound infections. The presence of resistant bacteria can delay wound healing and contribute to elevated rates of morbidity and mortality [4]. In light of these concerns, there is an urgent need to develop antimicrobial agents that are cost-effective and non-toxic to healthy tissues, while also capable of combating bacterial resistance [5].

Nanoparticles have found widespread use in biomedical research due to their antibacterial, antiviral, antioxidant, and anti-inflammatory properties [6]. Among the various methods, biosynthesis is favored due to its advantages, including greater efficiency, cleanliness, non-toxicity, cost-effectiveness, and sustainability [7]. Plants are naturally rich in redox-active phytochemicals, which can be extracted from various parts, including leaves, fruits, and seeds [8]. These plant extracts function both as reducing and capping agents, significantly reducing the reliance on harmful chemicals [9]. The process produces nanoparticles with consistent stability and uniformity, which can be optimized by altering key parameters such as pH, reaction time, temperature, and mixing ratios [10].

Silver (Ag) nanoparticles are well-known for their excellent antibacterial properties, making them a preferred material in the production of medical devices and textiles [10-11]. However, their performance is highly dependent on particle size, and reducing their size often leads to aggregation, which can reduce their antimicrobial potency. This aggregation is mainly due to their high surface energy and the strong attractive forces between particles [12]. Thus, Ag nanoparticles can be capped with metal oxides, such as zinc oxide (ZnO), creating a structure that enhances both surface area and stability. Additionally, combining multiple nanomaterials into a single hybrid nanocomposite can yield improved functionalities. These nanocomposites combine the distinct advantages of each component, resulting in superior performance compared to individual nanoparticles [13].

ZnO is widely recognized for its antibacterial properties against both pathogenic and non-pathogenic bacteria, as well as its chemical stability, large surface area, and non-toxic nature to human cells [14]. It plays a supportive role in Ag-based systems, where its synergistic interaction with Ag significantly enhances the antibacterial effectiveness of the combined nanocomposite [15]. The high chemical reactivity of ZnO, coupled with its large surface-to-volume ratio and reactivity, makes it well-suited for wet chemical analysis and particle adsorption applications, even at the micron scale [16]. Additionally, studies have demonstrated that ZnO nanoparticles synthesized through plant-based methods exhibit strong antibacterial properties [17].

Psidium guajava, particularly its leaves, is widely known for its medical properties, with research highlighting the presence of bioactive phytochemicals that offer therapeutic potential [18]. The therapeutic effects are largely due to polyphenols, including quercetin, the most prevalent flavonoid, as well as other flavonoids and phenolic acids such as ferulic, caffeic, and gallic acid [19]. Various studies have confirmed the effective synthesis of nanoparticles using guava leaf aqueous extracts, highlighting their diverse applications, particularly in antimicrobial and photocatalytic fields [18]. Building on this, the present research introduces a novel approach by employing an eco-friendly synthesis of ZnO/Ag nanocomposite using guava leaf extract, with primary focus on evaluating its antibacterial activity and exploring its innovative application in cotton bandages for enhanced wound healing treatment.

■ EXPERIMENTAL SECTION

Materials

The materials used in this study comprised of guava leaves, quercetin ($C_{15}H_{10}O_7$), 2% aluminum chloride ($AlCl_3$), 0.12 M potassium acetate (CH_3COOK), zinc acetate dihydrate ($Zn(CH_3COO)_2{\cdot}2H_2O$), silver nitrate ($AgNO_3$), 2 M sodium hydroxide (NaOH), hydrochloric acid (HCl), absolute ethanol (C_2H_5OH), phosphate-buffered saline (PBS), nutrient broth (NB), Mueller Hinton agar (MHA), universal pH indicator, Whatman No. 1, ampicillin antibiotic, *S. aureus* (ATCC 25923), and *E. coli* (ATCC 25922) bacterial suspension.

Instrumentation

Material characterization was carried out using a Fourier transform infrared spectrometer (FTIR, Shimadzu Prestige 21: Nicolet Avatar 360 IR), X-ray diffractometer (XRD, PANalytical), transmission electron microscope (TEM, JEOL JEM-1400), UV-visible-NIR spectrophotometer (Shimadzu UV 3600i Plus), and scanning electron microscope (SEM, JEOL JSM-6510). The guava leaf extract was analyzed using FTIR and UV-vis spectrophotometer (Shimadzu UV-1800) for functional groups and phytochemical characterization.

Procedure

Preparation of leaf extract

Fresh leaves were washed with tap water, rinsed with distilled water, and air-dried for 1 h, then ground into powder. As much as 10 g of the powder were boiled in 100 mL of distilled water at 90 °C for 25 min, then filtered twice using Whatman No.1 [20], yielding the guava leaf extract used in further experimental procedures.

Determination of total flavonoid content in leaf extract

The determination of total flavonoid content was carried out using a UV-vis spectrophotometer with

quercetin as the standard. The maximum wavelength was determined within the range of 400–800 nm. A standard curve for quercetin was prepared using standard solutions at concentrations of 10, 20, 30, 40, and 50 ppm. Meanwhile, the thick dry leaf extract was diluted in ethanol and reacted with 2% $AlCl_3$ and 0.12 M CH_3COOK. The resulting mixture was then measured at a wavelength of 425 nm.

Green synthesis of ZnO nanoparticles

The synthesis of ZnO nanoparticles was conducted following the procedure by Chauhan et al. [21], with several modifications. Firstly, a series of $Zn(CH_3COO)_2{\cdot}2H_2O$ with several precursor concentrations (0.30, 0.45, 0.60, 0.75, and 0.90 M) was made in distilled water and stirred for 30 min. The pH was adjusted to 12 to promote precipitation, followed by stirring at 50 °C for 30 min. Then, 10 mL of leaf extract was added, and the mixture was stirred continuously for 2 h. The mixture was filtered using Whatman No. 1, and the precipitate was washed with distilled water and ethanol. The precipitate was oven-dried at 60 °C for 24 h, ground, and calcined at 500 °C for 2 h, producing ZnO nanoparticles in the form of a fine white powder.

Green synthesis of ZnO/Ag nanocomposite

The synthesis of ZnO/Ag nanocomposites was also conducted with modifications to the procedure by Chauhan et al. [21]. Based on the previous stage, a 0.60 M solution of $Zn(CH_3COO)_2$ was prepared. A 1% $AgNO_3$ solution was added while maintaining the temperature at 50 °C for 10 min. The pH was adjusted to 12, and the mixture was stirred for 50 min. Then, 10 mL of leaf extract was added, and the reaction proceeded for 2 h. The mixture was filtered using Whatman No. 1, washed, oven-dried at 60 °C for 24 h, ground, and calcined at 500 °C for 2 h. To examine the effects of synthesis parameters, the procedure was repeated using different $AgNO_3$ concentrations (3 and 5%), reaction times (90 and 150 min), and neutral pH conditions to identify the optimal parameters. All materials were obtained as fine black ZnO/Ag nanocomposite (ZnO/Ag NCs) powders.

Application of ZnO and ZnO/Ag to cotton bandages

The coating of cotton bandages was performed using the ultrasonication method [22]. Here, 0.3 g ZnO and ZnO/Ag were dispersed in 30 mL of deionized water and subjected to ultrasonication for 10 min. A 1% NH_4OH solution was added dropwise until the pH reached 8, followed by an additional 10 min of ultrasonication. Cotton bandages were immersed in the prepared solution and further sonicated for 30 min. The coated cotton bandages were dried in an oven at 60 °C.

Antibacterial activity test

The antibacterial activity of ZnO, ZnO/Ag, and coated cotton bandages was evaluated using disk diffusion methods against *S. aureus* and *E. coli.* Initially, pure cultures of *S. aureus* and *E. coli* were taken and inoculated into conical tubes containing NB media. The cultures were then incubated at 37 °C for 24 h. MHA was poured into Petri dishes and left to solidify for several minutes. The incubated *S. aureus* and *E. coli* cultures were then evenly spread onto the surface of the MHA medium. Sterile paper discs were immersed in the 50 mg/mL samples suspension, positive control (ampicillin antibiotic), and negative control (PBS). These discs were then placed onto the surface of the MHA medium. It should be noted that for the sample of ZnO-coated cotton bandages, ZnO/Ag-coated cotton bandages, and uncoated cotton bandages were directly placed onto the MHA media without using paper discs. All petri dishes were incubated at 37 °C for 24 h, and the resulting inhibition zones were measured using a digital caliper.

■ RESULTS AND DISCUSSION

Guava leaves were chosen for this study owing to their therapeutic properties, primarily attributed to their high concentration of bioactive compounds. Bioactive compounds act as both reducing and capping agents, minimizing toxic by-products. In this case, bioactive compounds, such as polyphenols, characterized by hydroxyl groups in ortho or para positions on aromatic rings, readily oxidize to quinone while donating electrons to metal ions. The electron-rich atoms in the leaf extract facilitate the formation of ZnO from Zn^{2+} through controlled nucleation and subsequently reduce Ag^+ ions on ZnO nanoparticle surfaces to metallic Ag^0, while the oxidized quinone structures adsorb onto the

nanoparticle surface through hydrogen bonding and π–π interactions. This adsorbed layer acts as a capping layer, aiding in the stabilization and size regulation of the ZnO/Ag nanocomposite [23]. This selection was validated by an analysis of total flavonoid content, which revealed that the extract contained 84.28 mg QE/g.

Fig. 1 presents the FTIR spectra of ZnO and ZnO/Ag materials synthesized using Ag precursor concentrations of 1, 3, and 5%. A broad absorption band observed between 3500 and 3400 cm^{-1} in all samples is attributed to O–H stretching vibrations, indicating the presence of adsorbed water molecules and residual organic matter on the surface [12]. As the concentration of the Ag precursor increases, a noticeable shift to higher wavelengths is observed, suggesting the formation of stronger hydrogen bonds. The absorption peaks at 2924 and 1381 cm^{-1}, corresponding to C–H stretching and O–H bending modes, respectively, indicate the presence of organic residues from the guava leaf extract, further highlighting the role of plant-derived bioactive compounds in the green synthesis. The band around 439 cm^{-1} is characteristic of Zn–O bond vibrations, with slight shifts likely caused by the presence of Ag^{+} ions in the ZnO structure.

XRD analysis was performed on ZnO and ZnO/Ag synthesized under varying precursor concentrations, reaction times, and pH conditions, as it was selected as the primary analysis to determine the optimal synthesis conditions for this study. The ZnO diffraction peaks, shown in Fig. 2(a), appeared at 2θ values of 31.70°, 34.35°, 36.18°, 47.49°, 56.55°, 62.82°, 66.38°, 67.92°, and 69.04°, corresponding to the (100), (002), (101), (102), (110), (103), (200), (112), and (201) planes of a hexagonal wurtzite structure (COD No. 00-900-4181). The average crystal size of ZnO nanoparticles for precursor concentrations of 0.30, 0.45, 0.60, 0.75, and 0.90 M was 20.17, 19.07, 18.44, 20.98, and 20.67 nm, respectively, with 0.60 M identified as the optimal. A smaller crystallite size can provide a larger surface area, which may contribute to its improved antibacterial activity [24]. However, higher precursor concentrations can promote larger formation by increasing monomer supply and reducing diffusion distance [9].

The XRD analysis of ZnO/Ag nanocomposite (Fig. 2(b)) confirms the hexagonal structure of ZnO and the presence of Ag through distinct peaks at 2θ = 38.05°, 44.23°, and 64.40°, corresponding to the (111), (200), and (220) planes of Ag (COD No. 00-900-8459). The absence

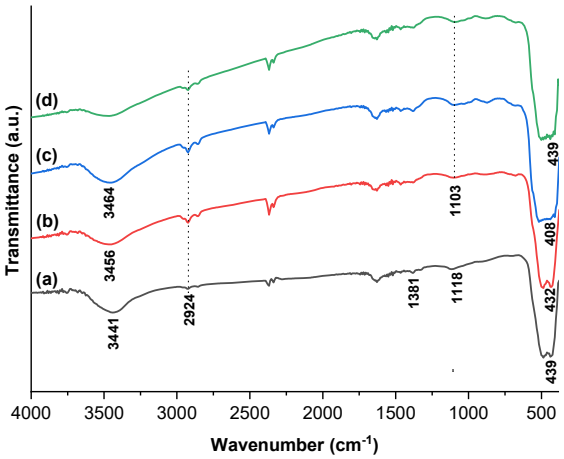

Fig 1. FTIR spectra of material (a) ZnO NPs, (b) ZnO/Ag NCs 1%, (c) ZnO/Ag NCs 3%, and ZnO/Ag NCs 5%

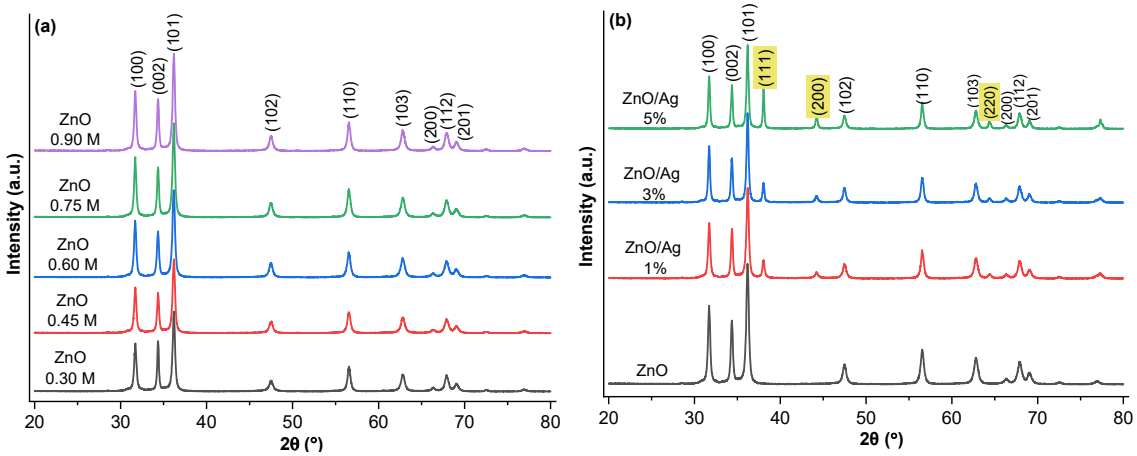

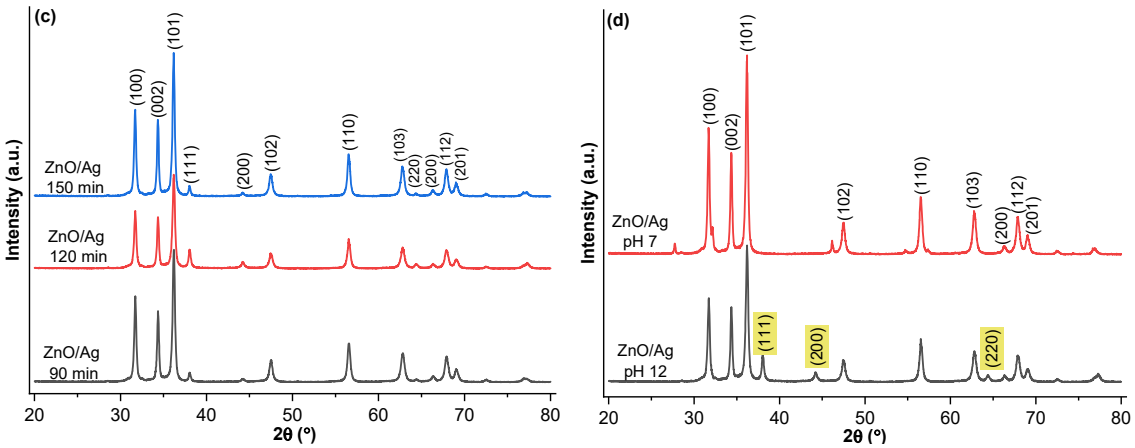

Fig 2. XRD pattern of (a) ZnO NPs in precursor concentration variation, (b) ZnO/Ag NCs in precursor concentration variation, (c) ZnO/Ag NCs in reaction time variation, and (d) ZnO/Ag NCs in pH variation

of notable peak shifts between pure ZnO and ZnO/Ag aligns with the observations of Alharthi et al. [25], suggesting that Ag is deposited on the ZnO surface rather than incorporated into its lattice, which can be attributed to the larger ionic radius of Ag^+ (1.22 Å) compared to Zn^{2+} (0.74 Å), which then hinders substitution. The average crystal sizes at 1, 3, and 5% Ag precursor concentrations were 20.07, 22.75, and 25.44 nm, respectively, indicating that 1% is the optimal level. In this case, the gradual increase in crystal size with higher Ag concentrations suggests that more Ag attaches to the ZnO surface, enhancing nucleation and surface energy during synthesis, which in turn promotes particle growth and leads to larger crystallite formation [26].

Fig. 2(c) displays the diffractogram of ZnO/Ag nanocomposites synthesized at reaction times of 90, 120, and 150 min, yielding average crystallite sizes of 22.05, 20.13, and 23.11 nm, respectively, which means that 120 min is the optimal duration. Longer reaction times can improve crystal uniformity and reduce agglomeration [27]. However, extended durations also reduce the free space between metal ions, increasing van der Waals interactions and causing particle clustering, which can lead to excessive growth and aggregation [9]. Moreover, Fig. 2(d) presents the diffraction patterns of ZnO/Ag nanocomposites synthesized at pH 7 and pH 12, with NaOH and HCl used to adjust pH. The absence of Ag peaks at pH 7 indicates Ag does not form in the ZnO structure under neutral conditions. This can be caused by the reactivity of plant-derived bioactive compounds, such as flavonoids, which varies with pH [28]. Under alkaline conditions, the higher abundance of phenolic functional groups enhances silver ion binding, promoting greater nanoparticle formation [29]. From all XRD results, the optimal ZnO/Ag nanocomposite synthesis conditions were established at 0.60 M ZnO precursor, 1% Ag precursor, 120 min reaction time, and pH 12, with the corresponding optimized nanocomposite subjected to further analyses.

Fig. 3(a–g) shows the SEM, EDX, and elemental mapping analyses of ZnO and ZnO/Ag samples. SEM observations reveal that Ag particles are not incorporated into the ZnO lattice but are instead deposited on the ZnO surface. This surface deposition results in morphological similarities between ZnO and Ag, making them visually distinguishable. The EDX spectrum of the ZnO material shows the presence of Zn and O, while the EDX spectrum of ZnO/Ag material confirms the presence of Zn, O, and Ag, verifying the successful synthesis of ZnO/Ag. Moreover, the lower Zn mass percentage in ZnO/Ag compared to pure ZnO suggests the presence of Ag in the ZnO structure. Mapping analysis of ZnO/Ag material shows a uniform distribution of Zn (light green), O (red), and Ag (dark green), confirming successful dispersion of Ag on the ZnO surface.

Additionally, Fig. 3(h–o) presents the SEM, EDX, and mapping characterization of the coated cotton bandages. The deposited particles exhibit rough and

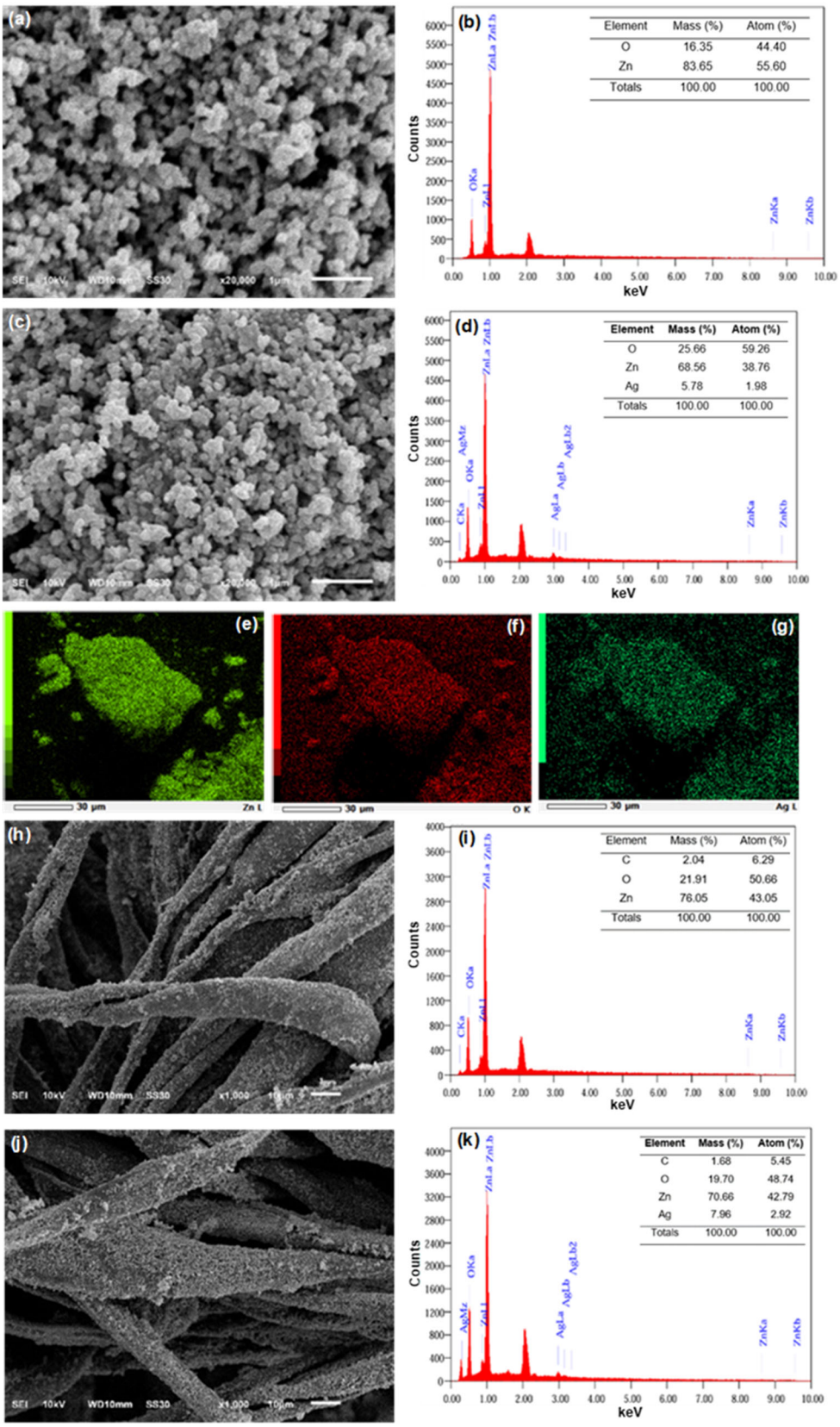
(a)
(b)
Element Mass (%) Atom (%)
O 16.35 44.40
Zn 83.65 55.60
Totals 100.00 100.00
Counts
keV
(c)
(d)
Element Mass (%) Atom (%)
O 25.66 59.26
Zn 68.56 38.76
Ag 5.78 1.98
Totals 100.00 100.00
Counts
keV
(e)
(f)
(g)
30 µm
Zn L
O K
Ag L
(h)
(i)
Element Mass (%) Atom (%)
C 2.04 6.29
O 21.91 50.66
Zn 76.05 43.05
Totals 100.00 100.00
Counts
keV
(j)
(k)
Element Mass (%) Atom (%)
C 1.68 5.45
O 19.70 48.74
Zn 70.66 42.79
Ag 7.96 2.92
Totals 100.00 100.00
Counts
keV

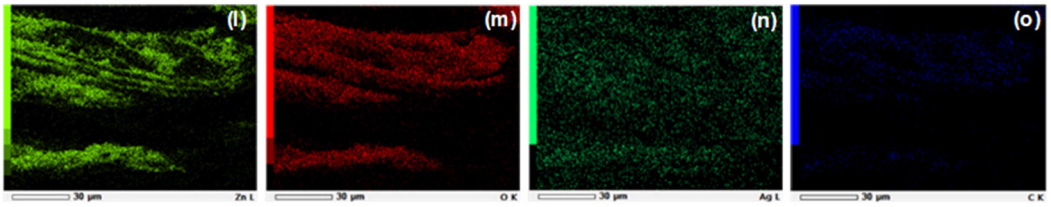

Fig 3. (a–b) SEM images and EDX of ZnO NPs, (c–g) SEM images, EDX, and mapping of ZnO/Ag NCs, (h–i) SEM images, and EDX of ZnO NPs-cotton, (j–o) SEM images, EDX, and mapping of ZnO/Ag NCs-cotton

irregular surface morphologies with slight agglomeration, likely due to excessive material deposition. Agglomeration is more pronounced in the ZnO-treated cotton bandages, while the ZnO/Ag-coated samples show a more uniform distribution of particles across the fiber surfaces. In addition to Zn, O, and Ag, the EDX spectrum also indicates the presence of C atoms from cellulose in the cotton fibers. Mapping analysis confirms the presence of Zn (light green), O (red), Ag (dark green), and C (blue), with minimal carbon intensity, indicating effective and uniform coating of the cotton bandages with the material.

The TEM image of ZnO nanoparticles, shown in Fig. 4(a), reveals predominantly hexagonal structures, along with some spherical, consistent with XRD and SEM results. Some aggregation is observed in ZnO material, likely due to polarity, electrostatic interactions, high surface energy, and particle compaction [30]. Moreover, calcination can also promote agglomeration by inducing a sintering effect during the synthesis process [31]. In Fig. 4(b), the ZnO/Ag material shows spherical Ag distributed on the ZnO surface. The nanocomposite consists primarily of hexagonal and spherical ZnO shapes, with some appearing ellipsoidal. Compared to pure ZnO, ZnO/Ag exhibits a more uniform particle distribution, as supported by SEM analysis. Additionally, the TEM histogram in Fig. 4(c–e) shows an average particle size of 72.54 nm for ZnO, 71.40 nm for ZnO in ZnO/Ag, and 17.75 nm for Ag. The reduced ZnO size in ZnO/Ag can be attributed to strong Ag^+ and ZnO interaction that influences nucleation and growth of particles [32]. The smaller ZnO particle size, more uniform distribution, and increased surface area resulting from Ag addition are expected to enhance antibacterial activity by providing more active sites for interaction with bacterial cells.

The optical properties of ZnO and ZnO/Ag were further investigated using UV-vis-NIR spectroscopy, with particular attention to their absorption spectra and estimated bandgap energy (E_g), as shown in Fig. 5(a–b). The result of the analysis reveals that ZnO shows a clear absorption peak at 361 nm, while the ZnO/Ag exhibits a noticeable redshift to 367 nm due to Ag deposition on the ZnO surface, which facilitates enhanced electron transitions from the valence to the conduction band [33-34]. This also corresponds to the E_g reduction from ZnO (3.02 eV) to ZnO/Ag (2.75 eV), which can be explained by the surface plasmon effect of Ag that enhances light absorption and electron excitation at the ZnO/Ag interface, leading to an apparent narrowing of the bandgap [35]. This enhanced photoexcitation, together with the difference in ionic radii between Ag and Zn,

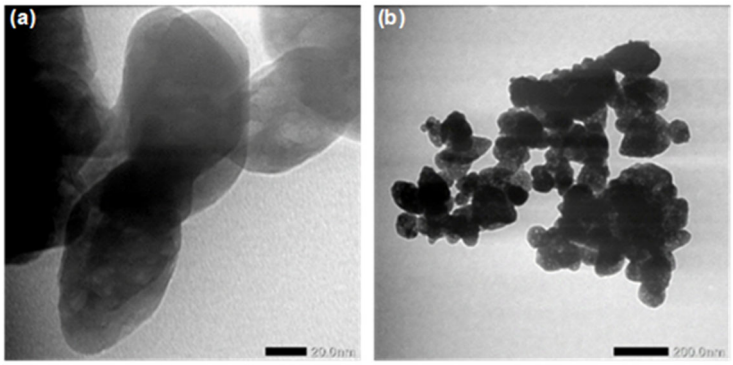

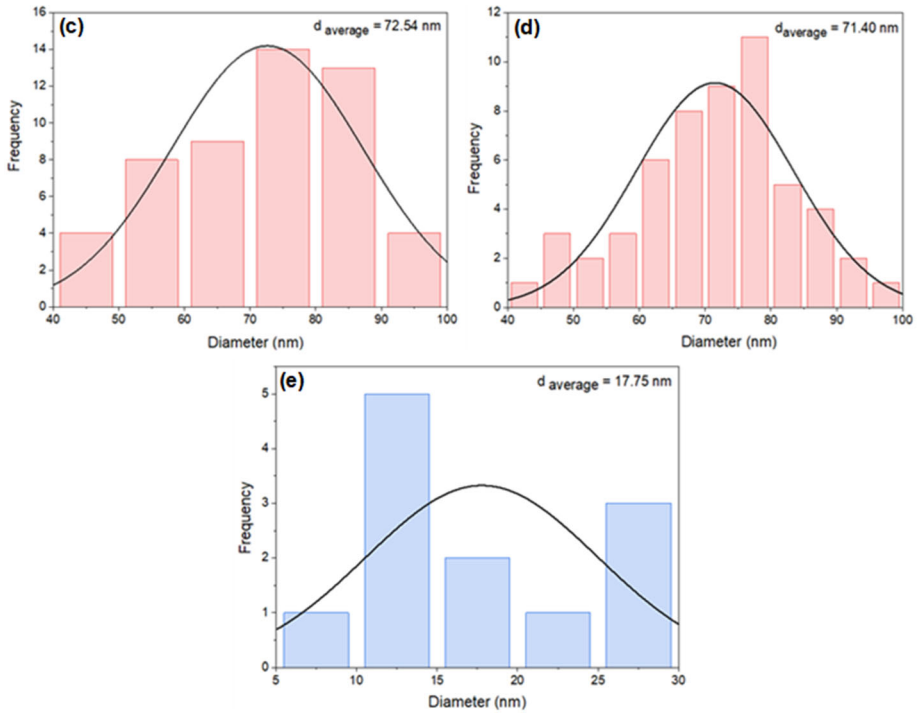

Fig 4. (a–b) TEM images of ZnO NPs and ZnO/Ag NCs, (c–d) particle distribution of ZnO NPs, ZnO in ZnO/Ag NCs, and Ag

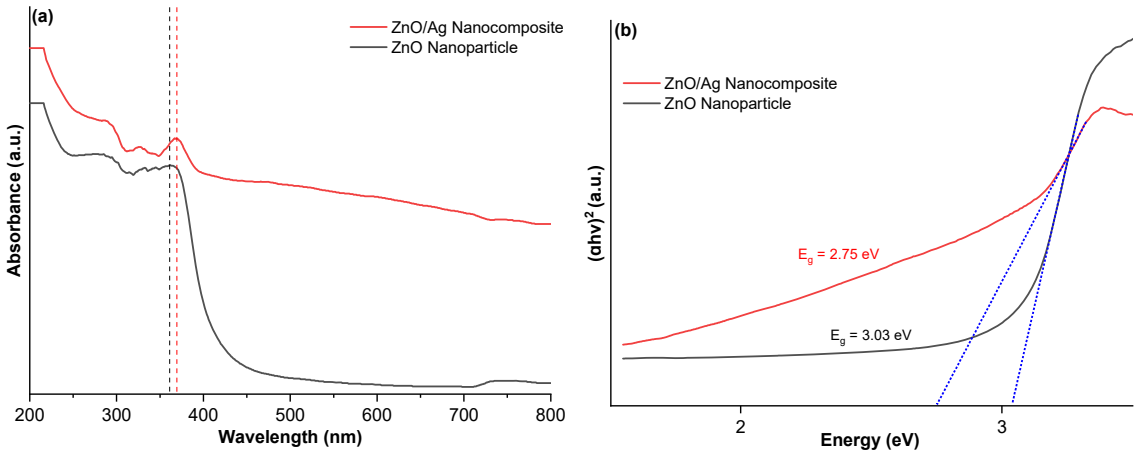

Fig 5. (a) UV-vis absorbance spectra and (b) Tauc plots for band gap quantification

improves charge separation, helps suppress electron-hole recombination, promotes free radical production, and ultimately boosts the antibacterial performance of the ZnO/Ag nanocomposite [33].

Antibacterial testing was conducted on ZnO nanoparticles, ZnO/Ag nanocomposites, and treated cotton bandages using the agar disk diffusion method. In this research, *E. coli* (Gram-negative bacteria) and *S. aureus* (Gram-positive bacteria) were selected as representative bacterial strains, with ampicillin as a positive control. Meanwhile, PBS and uncoated cotton bandages (for antibacterial testing of cotton bandages) served as negative controls. The antibacterial activity of ZnO and ZnO/Ag materials was assessed, with results summarized in Table 1. From the result, ZnO/Ag material showed stronger inhibition zones, particularly against *S. aureus*, while ZnO material exhibited no activity against *E. coli*, likely due to the concentration being too low and

Table 1. Inhibition zone of ZnO and ZnO/Ag material

Material	Inhibition zone (mm)					
	Control –	Control +	Sample	Control –	Control +	Sample
ZnO	-	25.90	14.55	-	5.90	-
ZnO/Ag	-	24.02	21.35	-	6.04	3.85
ZnO-cotton	-	-	14.30	-	-	-
ZnO/Ag-cotton	-	-	16.63	-	-	3.37

the higher resistance of gram-negative bacteria. This antibacterial activity is also connected to the size of the ZnO particle [36]. It can be seen from TEM results that ZnO in the ZnO/Ag is smaller than pure ZnO, and the presence of Ag particles further increases the surface area, which significantly enhances the antibacterial activity. These results are consistent across both direct material testing and coated cotton bandages, where ZnO/Ag-coated samples demonstrated superior antibacterial performance.

The absence of an inhibition zone for ZnO against *E. coli* implies that ZnO may have limited antibacterial efficacy toward this bacterium. Although this result contrasts with several studies reporting the performance of ZnO nanoparticles against *E. coli* [12,36], it is in agreement with other findings where ZnO showed no inhibitory effect on this bacterium [37-38]. This antibacterial activity can also be explained by the structural differences of bacterial cell walls, as their interaction with bacteria depends on the composition of the cell membrane [24]. According to a study by El-Habib et al. [39], *S. aureus* is more susceptible to ZnO nanoparticles compared to *E. coli*. This is because Gram-negative bacteria possess an outer membrane that shields their thin peptidoglycan layer, providing added protection. In contrast, Gram-positive bacteria have no outer membrane, leaving them more susceptible to membrane disruption and cell death. In addition, the observed reduction in inhibition zone diameter for coated cotton bandages compared to the material alone may be attributed to the strong chemical interactions between the material and cotton fibers, which can restrict mobility and slow release, thereby limiting direct interaction with the bacterial medium. Finally, the antibacterial test results, particularly coated cotton bandages with ZnO/Ag nanocomposite, highlight its potential for enhancing wound healing and support growing research on biosynthesized nanoparticles for clinical applications.

■ CONCLUSION

ZnO was successfully modified with Ag to synthesize a ZnO/Ag nanocomposite using guava leaf extract as a reducing and capping agent. The presence of phytochemical compounds facilitated the green synthesis process, demonstrating an environmentally friendly and sustainable approach. Characterization results confirm the successful formation of the ZnO/Ag nanocomposite, which exhibited enhanced antibacterial activity compared to pure ZnO. Antibacterial test of coated cotton bandages revealed their promising potential for biomedical applications. Specifically, ZnO/Ag-cotton showed superior antibacterial efficacy, with inhibition zones of 16.63 mm against *S. aureus* and 3.37 mm against *E. coli*. These findings highlight the potential of biosynthesized ZnO/Ag nanocomposites as effective materials for advanced wound dressing applications.

■ ACKNOWLEDGMENTS

The authors gratefully acknowledge the Faculty of Mathematics and Natural Sciences, Universitas Gadjah Mada, for their generous support, which significantly contributed to the success of this research. This work was supported under the 2025 Research Contract No. 3940/UN1/FMIPA.1.3/KP/PT.01.03/2025.

■ CONFLICT OF INTEREST

The authors confirm that there are no conflicts of interest that may have affected the conduct or findings of this research.

■ AUTHOR CONTRIBUTIONS

Yasmin Hasna Khairunnisa: conception and design, analysis, data collection and interpretation, drafting,

writing, and manuscript revision. Eko Sri Kunarti: supervision, conception and design, data analysis, review, and editing. Nuryono: data analysis, review, and editing.

■ REFERENCES

[1] Ali, A., Petrů, M., Azeem, M., Noman, T., Masin, I., Amor, N., Militky, J., and Tomková, B., 2023, A comparative performance of antibacterial effectiveness of copper and silver coated textiles, *J. Ind. Text.*, 52, 15280837221134990.

[2] Senthamarai Kannan, M., Hari Haran, P.S., Sundar, K., Kunjiappan, S., and Balakrishnan, V., 2022, Fabrication of anti-bacterial cotton bandage using biologically synthesized nanoparticles for medical applications, *Prog. Biomater.*, 11 (2), 229–241.

[3] Prastiyanto, M.E., Darmawati, S., Daryono, B.S., and Retnaningrum, E., 2024, Examining the prevalence and antimicrobial resistance profiles of multidrug-resistant bacterial isolates in wound infections from Indonesian patients, *Narra J.*, 4 (2), e980.

[4] Fitranda, M., Salasia, S.I.O., Sianipar, O., Dewananda, D.A., Arjana, A.Z., Aziz, F., Wasissa, M., Lestari, F.B., and Santosa, C.M., 2023, Methicillin-resistant *Staphylococcus aureus* isolates derived from humans and animals in Yogyakarta, Indonesia, *Vet. World*, 16 (1), 239–245.

[5] Nandhini, S.N., Sisubalan, N., Vijayan, A., Karthikeyan, C., Gnanaraj, M., Gideon, D.A.M., Jebastian, T., Varaprasad, K., and Sadiku, R., 2023, Recent advanced in green synthesized nanoparticles for bacterial and wound healing applications, *Heliyon*, 9 (2), e13128.

[6] Thandapani, G., Arthi, K., Pazhanisamy, P., John, J.J., Vinothini, C., Rekha, V., Santhanalakshmi, K., and Sekar, V., 2023, Green synthesis of copper oxide nanoparticles using *Spinacia oleracea* leaf extract and evaluation of biological applications: Antioxidant, antibacterial, larvicidal and biosafety assay, *Mater. Today Commun.*, 34, 1 105248.

[7] Hano, C., and Abbasi, B.H., 2022, Plant-based green synthesis of nanoparticles: Production, characterization and applications, *Biomolecules,* 12 (1), 31.

[8] Imade, E.E., Ajiboye, T.O., Fadiji, A.E., Onwudiwe, D.C., and Babalola, O.O., 2022, Green synthesis of zinc oxide nanoparticles using plantain peel extracts and the evaluation of their antibacterial activity, *Sci. Afr.*, 16, e01152.

[9] Monica Ahmad, N., Husaini Mohamed, A., Hasan, N.A., Zainal- Abidin, N., Zaini Nawahwi, M., and Mohamad Azzeme, A., 2024, Effect of optimisation variable and the role of plant extract in the synthesis of nanoparticles using plant-mediated synthesis approaches, *Inorg. Chem. Commun.*, 161, 111839.

[10] Vijayaram, S., Razafindralambo, H., Sun, Y.Z., Vasantharaj, S., Ghafarifarsani, H., Hoseinifar, S.H., and Raeeszadeh, M., 2024, Applications of green synthesized metal nanoparticles — A review, *Biol. Trace Elem. Res.*, 202 (1), 360–386.

[11] Liaqat, N., Jahan, N., ur-Rahman, K., Anwar, T., and Qureshi, H., 2022, Green synthesized silver nanoparticles: Optimization, characterization, antimicrobial activity, and cytotoxicity study by hemolysis assay, *Front. Chem.*, 10, 952006.

[12] Makauki, E., Mtavangu, S.G., Basu, O.D., Rwiza, M., and Machunda, R., 2023, Facile biosynthesis of Ag–ZnO nanocomposites using *Launaea cornuta* leaf extract and their antimicrobial activity, *Discover Nano*, 18 (1), 142.

[13] Mtavangu, S.G., Machunda, R.L., Bruggen, B., and Njau, K.N., 2022, *In situ* facile green synthesis of Ag–ZnO nanocomposites using *Tetradenia riperia* leaf extract and its antimicrobial efficacy on water disinfection, *Sci. Rep.*, 12 (1), 15359.

[14] Primo, J.O., Horsth, D.F., Correa, J.S., Das, A., Bittencourt, C., Umek, P., Buzanich, A.G., Radtke, M., Yusenko, K.V., Zanette, C., and Anaissi, F.J., 2022, Synthesis and characterization of Ag/ZnO nanoparticles for bacteria disinfection in water, *Nanomaterials*, 12 (10), 1764.

[15] Chand Gurjar, K., Agrawal, A., Kumar, S., Sharma, S., Sharma, R., Pandey, K., Pandey, H., and Awasthi, A., 2023, Antimicrobial efficacy of Ag-doped ZnO nanocomposite against *Bacillus subtilis*, *Mater. Today: Proc.*, 95, 61–66.

[16] Borysiewicz, M.A., 2019, ZnO as a functional material, A review, *Crystals*, 9 (10), 505.

[17] Kalra, K., Chhabra, V., and Prasad, N., 2022, Antibacterial activities of zinc oxide nanoparticles: A mini review, *J. Phys.: Conf. Ser.*, 2267 (1), 012049.

[18] Patil, S.P., and Rane, P.M., 2020, *Psidium guajava* leaves assisted green synthesis of metallic nanoparticles: A review, *Beni-Suef Univ. J. Basic Appl. Sci.*, 9 (1), 60.

[19] Kumar, M., Tomar, M., Amarowicz, R., Saurabh, V., Nair, M.S., Maheshwari, C., Sasi, M., Prajapati, U., Hasan, M., Singh, S., Changan, S., Prajapat, R.K., Berwal, M.K., and Satankar, V., 2021, Guava (*Psidium guajava* L.) leaves: Nutritional composition, phytochemical profile, and health-promoting bioactivities, *Foods*, 10 (4), 752.

[20] Islam, M.J., Khatun, N., Bhuiyan, R.H., Sultana, S., Ali Shaikh, M.A., Amin Bitu, M.N., Chowdhury, F., and Islam, S., 2023, *Psidium guajava* leaf extract mediated green synthesis of silver nanoparticles and its application in antibacterial coatings, *RSC Adv.*, 13 (28), 19164–19172.

[21] Chauhan, A., Verma, R., Kumari, S., Sharma, A., Shandilya, P., Li, X., Batoo, K.M., Imran, A., Kulshrestha, S., and Kumar, R., 2020, Photocatalytic dye degradation and antimicrobial activities of pure and Ag-doped ZnO using *Cannabis sativa* leaf extract, *Sci. Rep.*, 10 (1), 7881.

[22] Kachare, K., Shendage, S., Matwal, S., Walvekar, M., Vhanbatte, S., Chang, J.Y., and Ghule, A., 2024, Bio-mediated synthesized zinc oxide coated on cotton fabric for antibacterial and wound healing application, *Surf. Coat. Technol.*, 491, 131171.

[23] Mohamad Sukri, S.N.A., Shameli, K., Teow, S.Y., Chew, J., Ooi, L.T., Lee-Kiun Soon, M., Ismail, N.A., and Moeini, H., 2023, Enhanced antibacterial and anticancer activities of plant extract mediated green synthesized zinc oxide-silver nanoparticles, *Front. Microbiol.*, 14, 1194292.

[24] Wang, L., Hu, C., and Shao, L., 2017, The antimicrobial activity of nanoparticles: Present situation and prospects for the future, *Int. J. Nanomed.,* 12, 1227–1249.

[25] Alharthi, F.A., Alghamdi, A.A., Al-Zaqri, N., Alanazi, H.S., Alsyahi, A.A., El Marghany, A., and Ahmad, N., 2020, Facile one-pot green synthesis of Ag ZnO nanocomposites using potato peel and their Ag concentration dependent photocatalytic properties, *Sci. Rep.*, 10 (1), 20229.

[26] Thanh, N.T.K., Maclean, N., and Mahiddine, S., 2014, Mechanisms of nucleation and growth of nanoparticles in solution, *Chem. Rev.*, 114 (15), 7610–7630.

[27] Xiang, L., Fu, M., Wang, T., Wang, D., Xv, H., Miao, W., Le, T., Zhang, L., and Hu, J., 2024, Application and development of ultrasound in industrial crystallization, *Ultrason. Sonochem.*, 111, 107062.

[28] Ansari, M., Ahmed, S., Abbasi, A., Khan, M.T., Subhan, M., Bukhari, N.A., Hatamleh, A.A., and Abdelsalam, N.R., 2023, Plant-mediated fabrication of silver nanoparticles, process optimization, and impact on tomato plant, *Sci. Rep.*, 13 (1), 18048.

[29] Ndikau, M., Noah, N.M., Andala, D.M., and Masika, E., 2017, Green synthesis and characterization of silver nanoparticles using *Citrullus lanatus* fruit rind extract, *Int. J. Anal. Chem.*, 2017 (1), 8108504.

[30] Venkatesan, S., Suresh, S., Arumugam, J., Ramu, P., Pugazhenthiran, N., Jothilakshmi, R., and Prabu, K.M., 2024, Sunlight-assisted degradation of methylene blue dye by zinc oxide nanoparticles green synthesized using *Vitex negundo* plant leaf extract, *Results Chem.*, 7, 101315.

[31] Wintzheimer, S., Miller, F., Prieschl, J., Retter, M., and Mandel, K., 2019, Supraparticles with silica protection for redispersible, calcined nanoparticles, *Nanoscale Adv.*, 1 (11), 4277–4281.

[32] Rilda, Y., Puspita, F., Refinel, R., Armaini, A., Agustien, A., Pardi, H., and Sofyan, N., 2024, Biosynthesis of Ag-doped ZnO nanorods using template *Bacillus* sp. and polyethylene glycol via sol-gel-hydrothermal methods for antifungal application, *S. Afr. J. Chem. Eng.*, 47, 91–97.

[33] Rajendran, R., and Mani, A., 2020, Photocatalytic, antibacterial, and anticancer activity of silver-

doped zinc oxide nanoparticles, *J. Saudi Chem. Soc.*, 24 (12), 1010–1024.

[34] Cuadra, J.G., Scalschi, L., Vicedo, B., Guc, M., Izquierdo-Roca, V., Porcar, S., Fraga, D., and Carda, J.B., 2022, ZnO/Ag nanocomposite with enhanced antimicrobial, *Appl. Sci.*, 12 (10), 5023.

[35] Gea, S., Situmorang, S.A., Pasaribu, N., Piliang, A.F.R., Attaurrazaq, B., Sari, R.M., Pasaribu, K.M., and Goutianos, S., 2022, Facile synthesis of ZnO–Ag nanocomposite supported by graphene oxide with stabilised band-gap and wider visible-light region for photocatalyst application, *J. Mater. Res. Technol.*, 19, 2730–2741.

[36] Fakhirah, D., Maghfira, T.A., Hutama, A.S., Septama, A.W., Maryani, F., and Krismastuti, F.S.H., 2024, Synthesis, characterization, and antibacterial activity of plant-derived zinc oxide nanostructure using *Lavandula angustifolia* and *Phyllanthus niruri* extracts, *Indones. J. Chem.*, 24 (3), 865–875.

[37] Sharmila, C., Ranjith Kumar, R., and Chandar Shekar, C., 2018, *Psidium guajava:* A novel plant in the synthesis of silver nanoparticles for biomedical applications, *Asian J. Pharm. Clin. Res.,* 11 (1), 341–345.

[38] Karimi, E.Z., and Ansari, M., 2018, Comparison of antibacterial activity of ZnO nanoparticles fabricated by two different methods and coated on tetron fabric, *Open Biotechnol. J.*, 12, 166–175.

[39] El-Habib, I., Maatouk, H., Lemarchand, A., Dine, S., Roynette, A., Mielcarek, C., Traoré, M., and Azouani, R., 2024, Antibacterial size effect of ZnO nanoparticles and their role as additives in emulsion waterborne paint, *J. Funct. Biomater.*, 15 (7), 195.